Mechanical behavior of a DD5 single crystal superalloy with different misorientations under quasi-static and dynamic compression

Zhenpeng Liu, Hong Zhong,[a] Yumin Wang, Shuangming Li, and Hengzhi Fu
State Key Laboratory of Solidification Processing, Northwestern Polytechnical University, Xi'an 710072, People's Republic of China

(Received 31 January 2018; accepted 2 July 2018)

The effects of misorientation on the quasi-static and dynamic mechanical behaviors of a second generation Ni-based single crystal superalloy DD5 were investigated. A Split-Hopkinson pressure bar system was used to perform dynamic compression. The crystallographic misorientation between the stress axis and the [001] direction was characterized through rotating orientation X-ray diffraction. The results demonstrated that the flow stress was closely related to the misorientation. It decreased first and consequently increased as the misorientation increased from 0° to 45°. The dynamic flow stress was significantly higher than the quasi-static stress. Moreover, the flow stress under dynamics was more sensitive to the misorientation. A constitutive model was used to illustrate the misorientation effect on the mechanical behavior. Finally, the effect of strain rate on the crystal orientation was also investigated. It was discovered that the orientation deviation change following quasi-static compression could be neglected. By contrast, the orientation changed by 3–9° subsequently to dynamic compression.

I. INTRODUCTION

Nickel-based single crystal superalloys (SC-superalloys) have been widely utilized to gas turbine engine components, due to excellent strength and microstructure stability, as well as resistance to creep and fatigue at elevated temperatures.[1–3] Compared to polycrystalline materials, the SC-superalloy presents noticeable microstructural and mechanical property anisotropy.[4] Over the past years, many studies regarding the effect of crystallographic anisotropy on the mechanical properties of superalloys were conducted,[5–10] combining theoretical calculations and experimental data.

Earlier studies were mainly focused on the mechanical behaviors along the ⟨001⟩, ⟨011⟩, and ⟨111⟩ orientations. Certain alloys displayed the highest yield strength along the ⟨111⟩ orientation, such as the first generation PWA 1480 alloy at room temperature.[9] Certain SC-superalloys displayed the highest yield strength along the ⟨001⟩ orientation, such as the SRR99[8] and CMSX-4[10] alloys. The mechanical property anisotropy could be affected by the SC-superalloy composition. Furthermore, the ⟨001⟩-oriented single crystals are widely utilized due to their good mechanical properties at high temperature.[11,12]

A potential problem is, as turbine blades are produced with increasingly complex shapes, along with the addition of more heat resistant metal elements to improve the high temperature performance, the ⟨001⟩ orientation would be more difficult to grow strictly along the stress axis.[1,13] The blade performance deterioration is caused by apparent orientation deviation, even unavailability of SC-superalloy castings.[1] Consequently, researchers have begun to pay attention to the orientation deviation effect on the mechanical properties of SC-superalloys. The investigations regarding the misorientation from the ⟨001⟩ orientation were mainly concentrated on the high temperature creep and tensile properties. As an example, Matan et al.[14] discovered that the dispersions of rupture strength and lifetime increased as the deviation angle increased. Shah et al.[15] reported that the yield strength and ultimate tensile strength of the PWA1483 alloy exhibited a nearly linear decrease as the misorientation increased from 0° to 30°.

In recent years, more attention has been paid to the mechanical behavior of SC-superalloys under dynamic loading conditions compared to static loading. Wang et al.[16,17] utilized a Split-Hopkinson bar system (SHPB) to study the dynamic mechanical properties of DD407 and DD6 alloys at high strain rate $(\dot{\varepsilon} > 10^3\ s^{-1})$. It was observed that the ⟨001⟩-oriented SC-superalloy stress–strain response varied significantly with strain rate values ranging from $10^{-3}\ s^{-1}$ to $4 \times 10^3\ s^{-1}$. By contrast, the investigations regarding the mechanical behaviors at high strain rate were mainly concentrated on the [001] orientation. Dynamic mechanical behaviors along other orientations were rarely reported.

In this paper, the effect of misorientation on the SC-superalloy mechanical behavior at various strain rates

[a]Address all correspondence to this author.
e-mail: zhonghong123@nwpu.edu.cn
DOI: 10.1557/jmr.2018.251

 © Materials Research Society 2018

https://doi.org/10.1557/jmr.2018.251 Published online by Cambridge University Press

was focused on, especially at high strain rates. The effect of misorientation on the stress–strain response was analyzed. Moreover, the flow stress and orientation changes subsequently to deformation difference were discussed between the low and high strain rates.

II. EXPERIMENTAL PROCEDURE

A. Materials

The material in this study was selected to be a second generation single crystal nickel-based DD5 superalloy. The DD5 nominal chemical composition was Ni–7.0Cr–7.5Co–1.5Mo–5.0W–6.5Ta–3.0Re–6.2Al–0.15Hf–0.02C (wt%).[18] The single crystal with a nominal orientation [001] was cast in bars of roughly 16.5 mm in diameter and 15 cm in length, following directionally solidified in an industrial Bridgeman furnace through the grain selection technique.[18]

The directionally solidified microstructures of the DD5 SC-superalloys with a nominal [001] orientation are presented in Fig. 1. As it could be observed in Fig. 1 (a), the microstructure exhibited a typically dendritic structure with γ/γ' eutectic phase dispersion in the interdendritic regions (white region). Figures 1(b) and 1 (c) present the SEM micrograph of the DD5 SC-superalloy in the dendrite core and interdendritic regions, respectively. It could be observed that the alloy consisted of γ'-precipitates dispersed within the γ-matrix. The morphology of γ'-precipitates in the interdendritic regions was nearly regular cubic, while the mean size was approximately 380 nm, which was higher compared to the dendrite core (235 nm).

B. Cutting method of differently misoriented samples for testing

In this work, the effect of misorientation on the mechanical properties was mainly investigated. The samples for mechanical testing were cut from the bars in the as-cast state through electrical discharge machining, with various misaligned angles from [001] (angle between [001] orientation and axial direction). The detailed cutting method for the differently misoriented samples from [001] was conducted as follows: First, a cylinder of 20 mm in length was horizontally cut from the as-cast single bar. The cross section of the sample was mechanically ground, polished, and etched with a solution of 14 mL HCl, 21 mL H_2O, and 8 g $FeCl_3$ for optical observation. Second, a pair of second dendrite, with the same plane to the primary dendrite [(100) plane] was selected. The sample was cut parallel to the axial direction. Subsequently, the longitudinal section consisting of primary dendrites was gained and it was ground, polished, and etched. The primary dendrite direction, as the [001] orientation, was determined. Third, the differently misoriented angles (0°, 4.28°, 12.77°, 14.39°, 21.13°, 27.3°, and 45°) between the axial direction and the [001] orientation were calibrated. The wire direction was parallel to the calibrated direction. Finally, the samples differently misoriented from the [001] orientation were cut.

C. Quasi-static and dynamic tests

The samples were machined into cylinders of 5 mm in diameter and length and the ends of each specimen were carefully polished. Quasi-static compressive experiments were carried out with an Instron 3200 electromechanical testing machine at room temperature, with a nominal strain rate of 10^{-3} s^{-1}.

An enhanced SHPB[19] was utilized to perform dynamic compressive experiments at room temperature. The SHPB system consisted of the input and output bars of 12.8 mm in diameter, which were made of high strength steels. The specimens were located between the incident and transmit bars,[20] whereas consequently the incident bar was impacted by the striking bar. Subsequently to impact, the incident wave (ε_i), the reflective wave (ε_r), and the transmitted wave (ε_t) were detected at the strain gages and recorded with an oscilloscope. Based on the one-dimensional elastic-wave propagation theory, the compression strain (ε), the strain rate ($\dot{\varepsilon}$), and the stress (σ) of the specimens were calculated as follows[21,22]:

$$\varepsilon = \frac{-2C_0}{L}\int_0^t \varepsilon_r dt \quad , \tag{1}$$

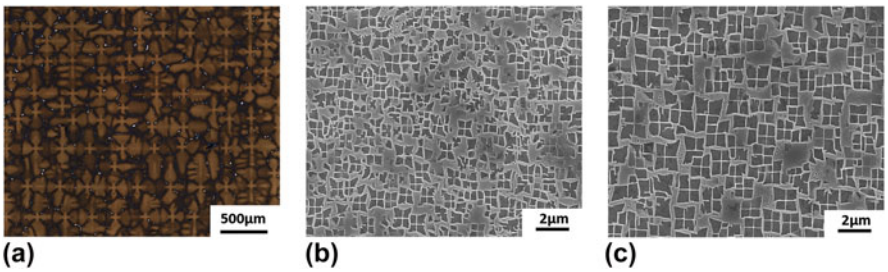


FIG. 1. Microstructure of DD5 SC-superalloys with [001] orientation, (a) dendrite structure, (b) SEM micrograph in the dendrite core, and (c) in interdendrite regions.

https://doi.org/10.1557/jmr.2018.251 Published online by Cambridge University Press

$$\dot{\varepsilon} = \frac{-2C_0}{L}\varepsilon_r \quad , \tag{2}$$

$$\sigma = \frac{EA}{A_s}\varepsilon_t \quad , \tag{3}$$

where C_0 is the longitudinal-wave velocity in the bar, L is the effective gage length of the specimen, E is the Young's modulus of the bar, and A and A_s are the cross-sectional areas of the split bar and specimen, respectively. Therefore the stress–strain curves upon compression could be attained. The nominal strain rate was approximately 3×10^3 s^{-1}.

D. Determination of orientation

The crystallographic orientations of the predeformed and deformed single crystals were analyzed with a RIGAKU D/MAX-2400 diffractometer with a Cu K_α source (Rigaku, Tokyo, Japan). The misorientation of a single crystal was evaluated with the rotating orientation X-ray diffraction (RO-XRD) method. A good match between electron backscattered diffraction (EBSD) and RO-XRD technologies exists for the misorientation measurements of SC-superalloys.[23] The RO-XRD method details could be observed in the Refs. 24 and 25. In this paper, EBSD was also utilized to acquire the pole and inverse pole figures of certain samples. The samples for EBSD examination were mirror-polished again and etched electrochemically to remove the deformed surface layers. EBSD measurements were carried out with a Tescan Mira 3 FEG SEM (Tescan, Brno, Czech Republic) enhanced with an Oxford Instruments HKL Nordly Max EBSD system (Oxford Instruments, London, United Kingdom). HKL Channel 5 software (Oxford Instruments, London, United Kingdom) was used for EBSD data processing and post analysis.

III. RESULTS

A. Misorientation of predeformed single crystal

Figure 2(a) presents the RO-XRD patterns of the [001]-oriented DD5 single crystal. Apparently, the patterns had only one diffraction peak, which implied that the [001] orientation was parallel to the axial direction of the samples. The XRD patterns of various misaligned [001] single crystals are depicted in Figs. 2(b)–2(f). It could be observed that the patterns of all the samples exhibited two diffraction peaks. This meant that the [001] orientations of the single crystals deviated from the axial direction. The deviation angle (θ) is calculated through the following equation[24]:

$$\theta = (\theta_2 - \theta_1)/2 \quad , \tag{4}$$

where θ_1 refers to the first diffraction peak angle and θ_2 refers to the second diffraction peak angle. The θ of the tested samples was measured as 0°, 4.28°, 12.77°, 14.39°, 21.13°, and 27.48°, respectively.

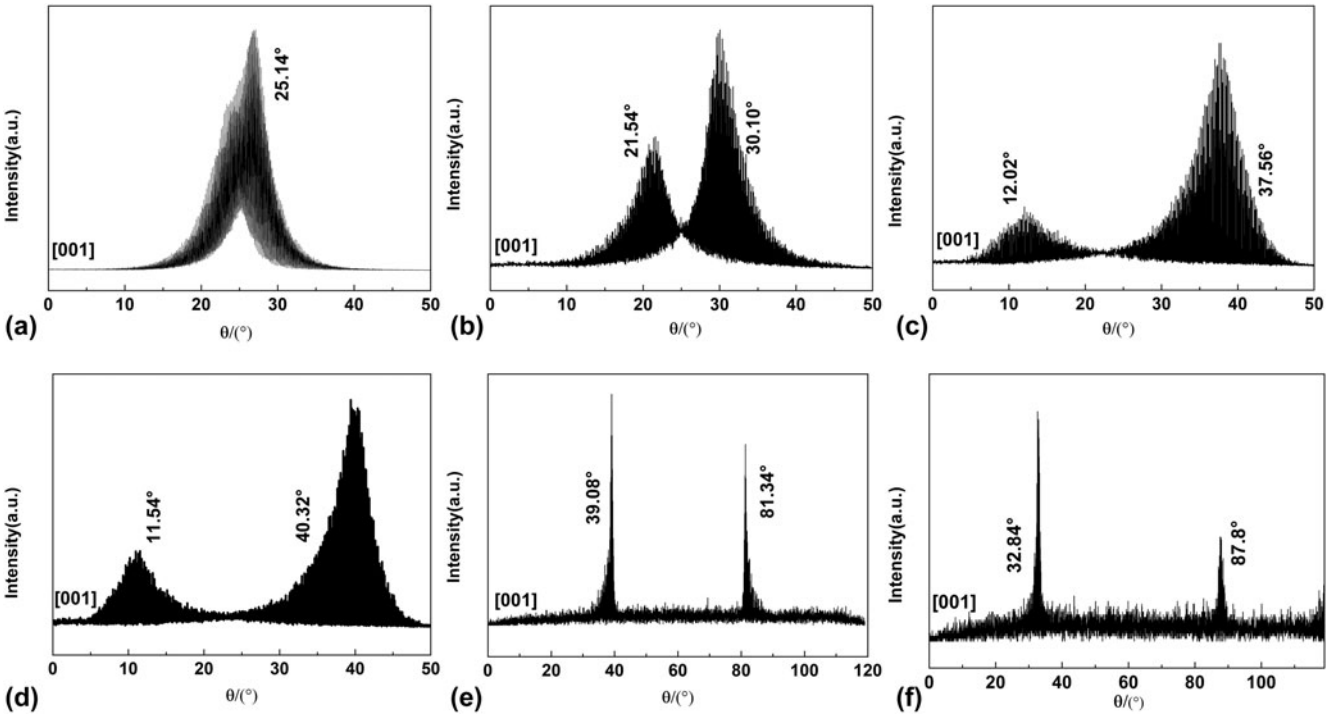


FIG. 2. RO-XRD patterns of the [001] DD5 single crystal with different misorientations: (a) θ = 0°, (b) θ = 4.28°, (c) θ = 12.77°, (d) θ = 14.39°, (e) θ = 21.17°, and (f) θ = 27.3°.

https://doi.org/10.1557/jmr.2018.251 Published online by Cambridge University Press

Based on the geometric principle, when the deviation angle between the [001] orientation and the axial is 45°, the single crystal orientation turns to the [011].[26] Consequently, the deviation angle of the [011]-oriented sample was measured at a fixed 2θ of the (220) diffraction plane. Figure 3 presents the XRD patterns of the [011]-oriented single crystal. Similarly, its patterns contained only one diffraction peak, which indicated that the sample had no deviation along the [011] direction.

B. Quasi-static compressive deformation behavior

Uniaxial quasi-static compression tests of the DD5 SC-superalloy were carried out at room temperature with the strain rate of 10^{-3} s^{-1}. The true stress–strain curves of differently misoriented single crystals are presented in Fig. 4(a). All stress–strain curves approximately exhibited elastic–plastic behavior. Also, the true stress is closely related to the true strain and misorientation.

Figure 4(b) presents the flow stress values under specific strain values. It could be observed that the flow stress decreased first as the deviation angle increased. When the deviation angle was approximately 22°, the flow stress reached the minimum. Following, the flow stress increased as the deviation angle increased. When the deviation angle was 45°, the maximum value was reached, while the corresponding crystallographic direction was [011]. Therefore, under the quasi-static condition of a 10^{-3} s^{-1} strain rate, the flow stress in the [011] direction was higher compared to the [001] direction. As an example, when the true strain was 0.15, the flow stress difference between the two crystallographic directions was approximately 70 MPa.

C. Dynamic compressive deformation behavior

Similarly, uniaxial dynamic compressions were conducted for the DD5 single crystal with various misorientations at room temperature with the strain rate of 3×10^3 s^{-1}. Figure 5(a) presents the true stress–strain curves. It was evident that the stress–strain curves approximately exhibited elastic–plastic behavior. The true stress was more dependent on misorientation compared to the quasi-static conditions.

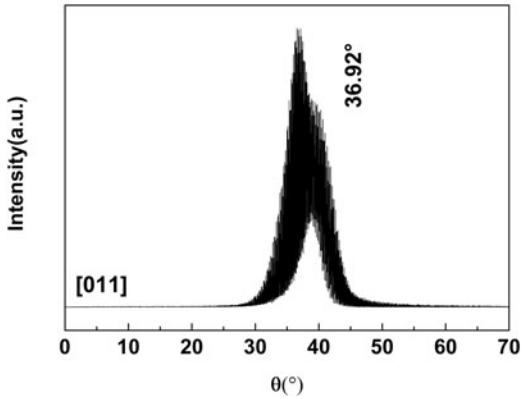


FIG. 3. RO-XRD patterns of [011]-oriented single crystal.

The flow stress values corresponding to certain true strains for various disoriented single crystals are presented in Fig. 5(b). Under the dynamic loading condition, the relation between misorientation and flow stress exhibited a similar phenomenon to the quasi-static loading condition. As the misorientation increased, the flow stress decreased at first and consequently increased. Compared to the quasi-static condition, the flow stress variation along with the misorientation was significantly apparent. This phenomenon was interpreted as a consequence of dislocation heterogeneity under high strain rate in FCC single crystals.[27] In addition, the flow stress along the [011] orientation was quite higher than along the [001] orientation. As an example, when the strain was 0.15, the flow stress difference between the two crystallographic directions was approximately 250 MPa.

It is worth noting that the flow stress difference corresponding to different misorientations is related to the strain value. As it could be observed from Fig. 4(b), when the strain was 0.1, the difference of flow stress between [001] and [011] orientations was approximately 34 MPa, whereas when the strain was 0.15, the flow stress difference was approximately 70 MPa. Under the high strain rate condition presented in Fig. 5(b), when the strain was 0.1, the flow stress difference between the [001] and [011] orientations was approximately 170 MPa; when the strain was 0.15, the flow stress difference was approximately 250 MPa. Consequently, as the true strain increased, the flow stress difference increased. This investigation was similar to a Ni_3Al single crystal investigation.[28]

IV. DISCUSSION

A. Effect of misorientation on compressive yield stress

The aforementioned experimental results indicated that the misorientation from [001] had a pronounced effect on the yield stress of the DD5 SC-superalloy. The yield stress versus misorientation relation was reported for the PWA1480 superalloy.[29,30] The relation was caused by unequal Schmid factors along different orientations. In general, a SC-superalloy deforms through the $\{111\}\langle 011\rangle$ slip system opening at room temperature. The yield strength depends on the critical shear strength of opened slip-systems.[29] When the crystallographic orientation is [001], the critical shear strength of a single crystal is calculated through the following equation based on the Schmid Law:

https://doi.org/10.1557/jmr.2018.251 Published online by Cambridge University Press

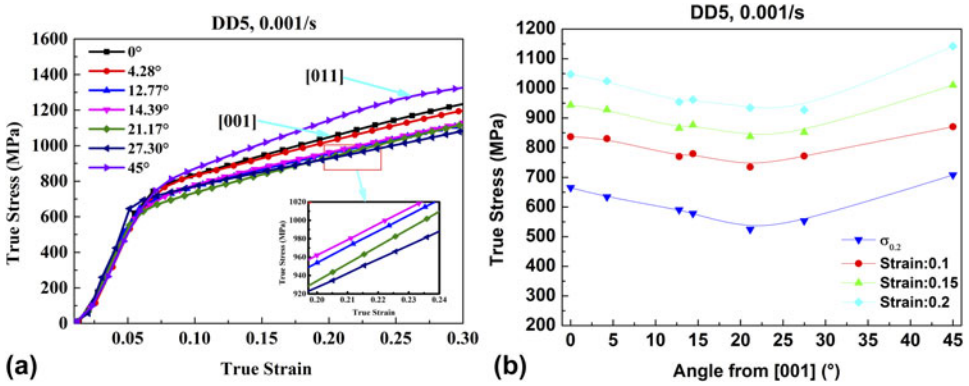


FIG. 4. (a) True stress strain curves and (b) relationship between flow stress and misorientation at different strain values, at the nominal strain rate of 10^{-3} s^{-1} for the DD5 single crystal.

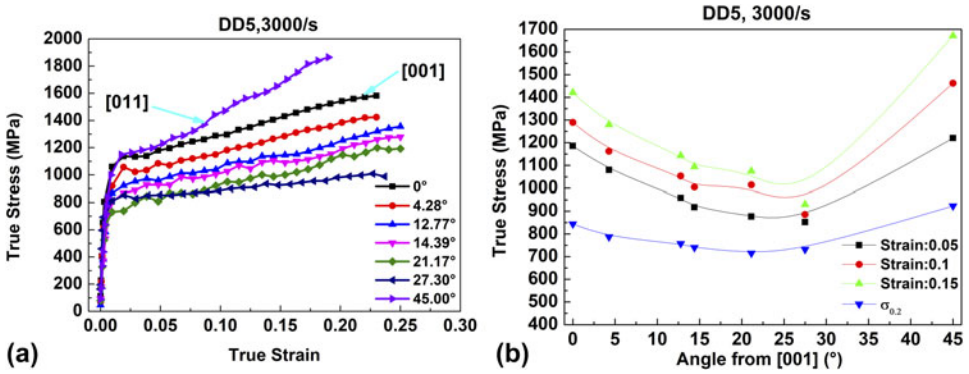


FIG. 5. (a) True stress strain curves and (b) relationship between flow stress and misorientation at different strain values, at the nominal strain rate of 3×10^{3} s^{-1} for the DD5 single crystal.

$$\tau = \sigma_y \Omega = \sigma_y \cos\varphi \cos\lambda \quad , \tag{5}$$

where τ is the critical shear strength; σ_y is the yield strength; Ω is the Schmid factor; φ is the angle between the axial direction and the normal direction of slip planes, while λ is the angle between the axial direction and the slip line direction. It is well known that the number of slip systems has a profound on the mechanical behaviors, especially the plasticity. Adversely, a SC-superalloy is deformed by only one or two octahedral slip systems prior to yielding.[31,32] For all misoriented samples in this investigation, the Schmid factor was identical for all octahedral slip systems within a certain orientation. Consequently, it could be assumed that the specific $(111)[10\bar{1}]$ slip system was activated and selected to simulate the Schmid factor in the following discussion. As it could be observed in Ref. 30, the Schmid factor of a [001]-oriented single crystal is 0.41. As the deviation angle increases, the Schmid factor increases first and consequently decreases. The yield strength is inversely proportional to the Schmid factor; therefore, the yield strength decreases first and consequently increases as the misorientation increases.

In addition, the [011] and [001] orientations have the same Schmid factors. If only the $(111)[10\bar{1}]$ slip system is considered, the yield strength of these two directions should be consistent from Eq. (5). Adversely, in the current test results, the compressive yield strength in the [011] direction was always higher compared to the [001] direction. This occurred due to the different cross-slip probabilities in the SC-superalloy. The parameter N represents the cross-slip extent.

$$N = \frac{\text{Schmid factor } (010)[\bar{1}01]}{\text{Schmid factor } (111)[\bar{1}01]} \quad . \tag{6}$$

Through calculations, the N value along near [011] orientation was higher than near the [001]. Therefore, the near [011] orientation was more likely to cross-slip, which impeded the octahedral slip. Consequently, the yield strength along the [011] orientation was higher.

Due to the matrix phase γ and strengthening phase γ' coexistence, the strengthening mechanism of the SC-superalloy was quite complex. In many studies, certain constitutive models were established to describe the relationship between flow stress and crystallographic orientation under various experimental conditions.

https://doi.org/10.1557/jmr.2018.251 Published online by Cambridge University Press

On the basis of slip plane observation through TEM, in many studies,[29,33,34] it was suggested that the main deformation mechanism of the Ni-based superalloy along the [001] and [011] orientations was the octahedral slip system, when the temperature was below 873 K. Lall, Chin, and Pope proposed a model (LCP-model)[35] to describe the critical resolved shear stress anisotropy of an SC-superalloy at the given temperature and strain rate. Also, a good agreement in yield strength values between the simulated values through the LCP model and the experimental results existed in the SC16 and Nimonic 105 alloys.[29] The LCP-model equation is

$$S_1\sigma_y = T_n + A_0 \exp\left[\left(-H_0 + A_2S_2\sigma_y + \delta A_3S_3\sigma_y\right)/RT\right] \quad , \tag{7}$$

where the Schmid factors $S_1 = S_{(111)[\bar{1}01]}$, $S_2 = S_{(010)[\bar{1}01]}$, A_0, A_2, A_3 are constants, T is the temperature, and T_n is the resolved shear stress under a specified temperature. In the equation, the exponent of $\exp\left[\left(A_2S_2\sigma_y + \delta A_3S_3\sigma_y\right)/RT\right]$ is relatively low and it could be approximated as $1 + \left(A_2S_2\sigma_y + \delta A_3S_3\sigma_y\right)/RT$ through the Taylor expansion at a zero point. Following a rearrangement of terms, the variables are separated in the form:

$$1/\sigma_y = b_1S_1 + b_2S_2 + \delta b_3S_3 \quad , \tag{8}$$

where $b_1 = 1/[T_n + A_0 \exp(-H_0/RT)]$, $b_2 = (-b_1A_0A_2/RT)/\exp(-H_0/RT)$, and $b_3 = (-b_1A_0A_3/RT)/\exp(-H_0/RT)$. δ is $+1$ for tensile loading and -1 for compressive loading. In this form, the orientation dependence of σ_y at a given strain rate could be numerically evaluated through regression analysis.

The Schmid factors and the compressive yield strength values of specimens with different misorientations are listed in Table I. Through multiple regression analysis according to Eq. (8) with the authors' experimental results, the fitting constants were obtained. Under the quasi-static loading condition, $b_1 = 3.46 \times 10^{-3}$, $b_2 = 0.36 \times 10^{-3}$, and $b_3 = 0.50 \times 10^{-3}$, while under the dynamic condition, $b_1 = 2.8 \times 10^{-3}$, $b_2 = -0.032 \times 10^{-3}$, and $b_3 = 0.26 \times 10^{-3}$. The b_1 term represents the primary octahedral slip. For the dynamic condition, insufficient time existed for the dislocation to slip, consequently leading to dislocation pile-up at the γ/γ' interface. Subsequently, the b_1 was lower under the dynamic condition than under the quasi-static condition. Miner et al.[33] argued that the b_2 term (cross-slip term) could be neglected under lower temperature. In the authors' results, the b_2 was positive under quasi-static conditions, which coincided with the SC16 and René N4 alloys according to the experimental results by Miner et al.[33] and Österle et al.[29] Adversely, the b_2 becomes negative under dynamic conditions. Österle et al.[29] considered that the b_2 term consisted of two parts; one part was the negative term caused by the cube cross-slip, while the other part was positive, as derived from the shear deformation of the γ matrix channel. In the present result, it could be considered that the shear deformation extent of the γ matrix was higher than the cube cross-slip probability, leading to the b_2 term positive value under quasi-static loading. Moreover, the b_2 negative value was caused by the higher probability of the cube cross-slip under dynamic loading.

To check the validity of the LCP, the yield strength was calculated:

$$\sigma_y = (3.46S_1 + 0.36S_2 - 0.5S_3)^{-1} \times 10^3 \quad , \tag{9}$$

$$\sigma_y = (2.80S_1 - 0.032S_2 - 0.26S_3)^{-1} \times 10^3 \quad . \tag{10}$$

The yield strength calculated according to Eqs. (9) and (10) is plotted in Fig. 6. For comparison, the experimental results of the DD5 SC-alloy are also presented. The experimental values were in good agreement with the calculated values, which could display the misorientation effect on the yield strength.

TABLE I. Schmid factors of different misorientations and yield strength of corresponding specimens under quasi-static and dynamic compression.

				Yield strength (MPa)	
Misorientation (°)	S_1	S_2	S_3	Quasi-static	Dynamic
0	0.425	0.030	0.021	665	844
4.28	0.433	0.058	0.175	634	787
12.77	0.452	0.135	0.107	590	757
14.39	0.483	0.178	0.128	578	740
21.13	0.493	0.254	0.043	524	715
27.48	0.497	0.295	−0.012	553	732
45	0.413	0.353	−0.227	708	913

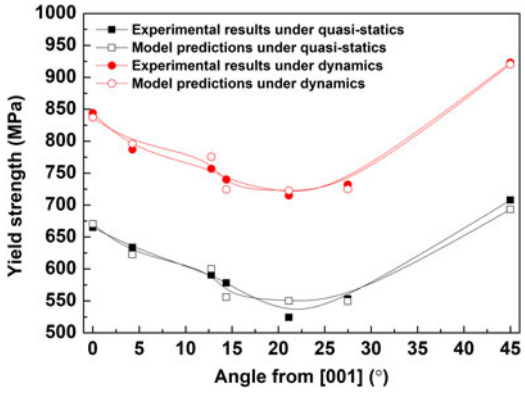


FIG. 6. Relationship between yield strength and crystallographic misorientation, comparison of LCP model predictions with experimental results.

https://doi.org/10.1557/jmr.2018.251 Published online by Cambridge University Press

B. Comparison of flow stress between quasi-static and dynamic compression

The flow stress values from quasi-static and dynamic compression were compared with specimens of different crystallographic misorientation values (0°, 12.77°, 21.13°, and 45°). It could be observed from Fig. 7(a) that the difference in yield strength between dynamic and quasi-static compression was approximately 200 MPa.

As it could be observed from Figs. 7(b) and 7(c), at a strain value of 0.1, the difference in flow stress along the [011] orientation between dynamic and quasi-static compression was nearly 590 MPa. At a strain value of 0.15, the difference was approximately 660 MPa. The flow stress under dynamic condition was significantly higher compared to quasi-static flow stress.

It could also be observed from Fig. 7 that the misorientation had a more pronounced effect on the flow stress at high strain rates. In Fig. 7(b), the flow stress along the [011] orientation (45°) was improved by 4.02% than at the [001] orientation (0°) at a strain rate of 10^{-3} s^{-1} and improved by 13.3% at a strain rate of 3×10^{3} s^{-1}. Moreover, in Fig. 7(c), the flow stress along the [011] orientation (45°) was improved by 7.2% than that at the [001] orientation at a strain rate of 10^{-3} s^{-1} and improved by 17.7% at a strain rate of 3×10^{3} s^{-1}.

C. Crystal orientation deviation following compressive deformation

Subsequent to quasi-static and dynamic compression, the crystallographic orientation deviations of the single crystal samples were measured through the RO-XRD method. Compared to the undeformed sample, not only under quasi-static compression but also under dynamic compression, the nominal orientation had not changed, whereas only the diffraction angle changed slightly. The deviation angle obtained through RO-XRD testing is presented in Table II.

Following quasi-static compression, the misorientation of the single crystal varied from 0°, 4.28°, 12.77°, 14.39°, 21.13°, and 27.30° to 0°, 4.30°, 14.08°, 14.32°, 22.09°, and 25.47°. By contrast, the misorientation of single crystal changed to 5.99°, 10.55°, 21.47°, 22.69°, 24.97°, and 31.01° subsequently to dynamic compression. It was evident that under high strain rate compression, the orientation difference of the single crystal samples was quite higher than that under quasi-static loading. For the sample with a misorientation of 12.77°, following quasi-static compression, the orientation deviation between the sample and the [001] direction was 14.08°, increased by 10.3%, while the orientation deviation was 21.47°, increased by 68.1% following dynamic compression.

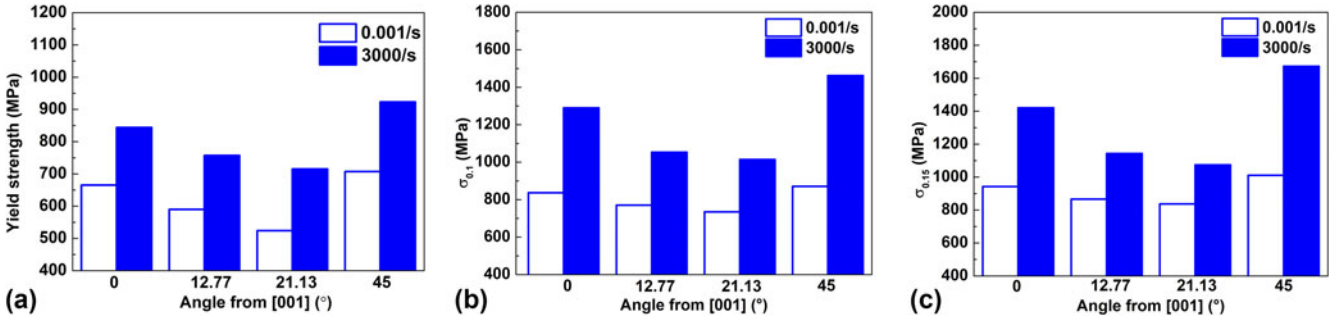


FIG. 7. Compressive flow stress at different strain rates (10^{-3} s^{-1} and 3×10^{3} s^{-1}) and crystallographic misoreintation: (a) Yield strength, (b) true stress at $\varepsilon = 0.1$, and (c) true stress at $\varepsilon = 0.15$.

TABLE II. Misorientation of samples after quasi-static and dynamic compression.

		Quasi-static compression				Dynamic compression			
Misorientation	Crystal orientation	θ_1	θ_2	θ	$\Delta\theta$	θ_1	θ_2	θ	$\Delta\theta$
0°	[001]	27.52°	...	0°	0°	20.09°	32.06°	5.99°	5.99°
4.28°	[001]	20.56°	29.16°	4.30°	0.02°	13.98°	35.02°	10.55°	5.27°
12.77°	[001]	12.96°	41.12°	14.08°	1.31°	4.34°	47.28°	21.47°	8.70°
14.39°	[001]	11.36°	40.0°	14.32°	−0.07°	37.50°	82.88°	22.69°	8.30°
21.17°	[001]	37.46°	81.64°	22.09°	0.92°	36.80°	86.74°	24.97°	3.82°
27.30°	[001]	34.48°	85.42°	25.47°	−1.83°	29.02°	91.04°	31.01°	3.71°
45.00°	[011]	36.92°	...	0°	0°	35.82°	39.98°	2.08°	2.08°

https://doi.org/10.1557/jmr.2018.251 Published online by Cambridge University Press

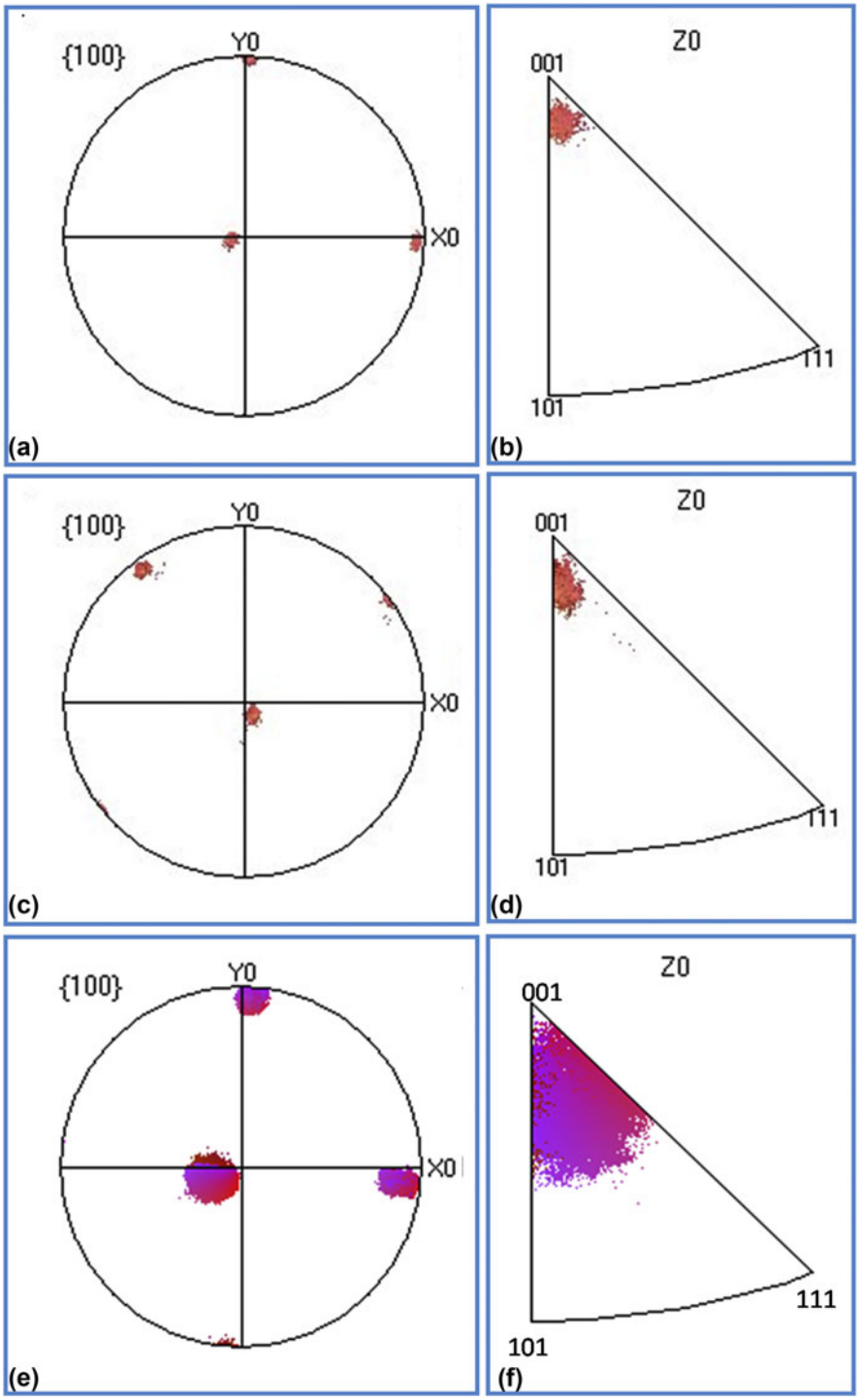


FIG. 8. (a), (c), and (e) {001} pole figures and (b), (d), and (f) inverse pole figures of the ⟨001⟩ oriented sample, (a) and (b) before deformations, (c) and (d) after quasi-static deformations (e) and (f) after dynamic deformations.

Figure 8 presents the pole figure and inverse pole figure of the [001] orientation sample prior to and following quasi-static and dynamic compression. Prior to compression, the single crystal orientation was mainly near the [001] orientation. Following quasi-static compression, the orientation dispersion had no more changes but became more apparent subsequently to dynamic loading, as presented in Figs. 8(c) and 8(d). Therefore, the reason for the higher misorientation change subsequently to dynamic compression might be the higher orientation dispersion.

https://doi.org/10.1557/jmr.2018.251 Published online by Cambridge University Press

V. CONCLUSIONS

In this study, the mechanical behavior of DD5 single crystals with different misorientations was investigated under quasi-static and dynamic compression at room temperature. The conclusions drawn from this study were as follows:

(1) Through the experimental and modeling results, the yield strength and the flow stress of the DD5 SC-superalloys exhibited apparent anisotropy and similar trends: first a decrease and consequently an increase as the deviation angle increased within the misorientation of 0–45° under all the strain rates. This was related to the different Schmid factors for different misorientations.

(2) The yield strength and the flow stress of the DD5 SC-superalloy along the [011] orientation were higher compared to the [001] orientation.

(3) The yield strength and the flow stress under dynamic compression were higher compared to the quasi-static compression. Also, under high strain rate, the flow stress was more sensitive to the misorientation of single crystals.

(4) The misorientation changed subsequently to compressive deformations. In quasi-static compression, the degree of the misorientation was negligible, of approximately 1–2°. Adversely, the misorientation degree change was more apparent, of 3–9° following dynamic compression.

ACKNOWLEDGMENTS

The authors wish to thank Tao Suo for performing SHPB experiments. This work was supported by the National Natural Science Foundation of China (No. 51674201), the Fundamental Research Funds for the Central Universities (3102014JCQ01021), and the Research Fund of the State Key Laboratory of Solidification Processing (NWPU), China (No. 101-QP-2014).

REFERENCES

1. R.C. Reed: *The Superalloys: Fundamentals and Applications* (Cambridge University Press, Cambridge, 2006); p. 139.
2. P. Zhang, Y. Yuan, Z. Gao, B. Li, G. Yang, and X. Song: Plastic deformation mechanisms in a new Ni-base single crystal superalloy at room temperature. *J. Microsc.* **268**, 186 (2017).
3. L. Roux, H. Chalons, H. Maigre, and D. Nelias: High strain rate behavior of MC2 single crystal under uniaxial compression load at high temperature: Experiments and modeling. *Mech. Mater.* **104**, 145 (2017).
4. X.B. Zhao, L. Liu, Z.H. Yu, W.G. Zhang, and H.Z. Fu: Microstructure development of different orientated nickel-base single crystal superalloy in directional solidification. *Mater. Charact.* **61**, 7 (2010).
5. L.X. Tian, J. Chen, W.L. Xiao, and C.L. Ma: Orientational dependence of microstructure evolution and the related deformation mechanism of a single crystal Ni-base superalloy. *Mater. Sci. Eng., A* **684**, 115 (2017).
6. Z.J. Zhou, L. Wang, D. Wang, L.H. Lou, and J. Zhang: Effect of secondary orientation on room temperature tensile behaviors of Ni-base single crystal superalloys. *Mater. Sci. Eng., A* **659**, 130 (2016).
7. D. Leidermark, J.J. Moverare, K. Simonsson, S. Sjöström, and S. Johansson: Room temperature yield behaviour of a single-crystal nickel-base superalloy with tension/compression asymmetry. *Comput. Mater. Sci.* **47**, 366 (2009).
8. L.N. Wang, Y. Liu, J.J. Yu, Y. Xu, X.F. Sun, H.R. Guan, and Z.Q. Hu: Orientation and temperature dependence of yielding and deformation behavior of a nickel-base single crystal superalloy. *Mater. Sci. Eng., A* **505**, 144 (2009).
9. R.P. Dalal, C.R. Thomas, and L.E. Dardi: The effect of crystallographic orientation on the physical and mechanical properties of an investment cast single crystal nickel-base superalloy. In *Superalloys*, W.B.K.R.H. Bricknell, M. Gell, C.S. Kortovich, and J.F. Radavich, eds. (TMS, Warrendale, Pennsylvania, 1984); p. 185.
10. A. Vattré and B. Fedelich: On the relationship between anisotropic yield strength and internal stresses in single crystal superalloys. *Mech. Mater.* **43**, 930 (2011).
11. A. Vattré, B. Devincre, and A. Roos: Orientation dependence of plastic deformation in nickel-based single crystal superalloys: Discrete–continuous model simulations. *Acta Mater.* **58**, 1938 (2010).
12. P. Zhang, Y. Yuan, B. Li, S.W. Guo, G.X. Yang, and X.L. Song: Tensile deformation behavior of a new Ni-base superalloy at room temperature. *Mater. Sci. Eng., A* **655**, 152 (2016).
13. Y.Z. Zhou, A. Volek, and R.F. Singer: Effect of grain boundary characteristics on hot tearing in directional solidification of superalloys. *J. Mater. Res.* **21**, 2361 (2006).
14. N. Matan, D.C. Cox, P. Carter, M.A. Rist, C.M.F. Rae, and R.C. Reed: Creep of CMSX-4 superalloy single crystals: Effects of misorientation and temperature. *Acta Mater.* **47**, 1549 (1999).
15. D.M. Shah and A. Cetel: Evaluation of PWA1483 for large single crystal IGT blade applications. In *Superalloys*, T.M. Pollock, R.D. Kissinger, and R.R. Bowman, eds. (TMS, Warrendale, Pennsylvania, 2000); p. 295.
16. J.J. Wang, W.G. Guo, Y. Su, P. Zhou, and K.B. Yuan: Anomalous behaviors of a single-crystal nickel-base superalloy over a wide range of temperatures and strain rates. *Mech. Mater.* **94**, 79 (2016).
17. J.J. Wang, W.G. Guo, P.H. Li, P. Zhou, and Z.Q. Wang: Dynamic tensile properties of a single crystal nickel-base superalloy at high temperatures measured with an improved SHTB technique. *Mater. Sci. Eng., A* **670**, 1 (2016).
18. R.J. Cui and Z.H. Huang: Microstructual evolution and stability of second generation single crystal nickel-based superalloy DD5. *Trans. Nonferrous Met. Soc. China* **26**, 2079 (2016).
19. T. Suo, Y-l. Li, K. Xie, F. Zhao, K-S. Zhang, and Q. Deng: Experimental investigation on strain rate sensitivity of ultra-fine grained copper at elevated temperatures. *Mech. Mater.* **43**, 111 (2011).
20. C. Zhang, T. Suo, W. Tan, X. Zhang, J. Liu, C. Wang, and Y. Li: An experimental method for determination of dynamic mechanical behavior of materials at high temperatures. *Int. J. Impact Eng.* **102**, 27 (2017).
21. S. Abotula, A. Shukla, and R. Chona: Dynamic constitutive behavior of Hastelloy X under thermo-mechanical loads. *J. Mater. Sci.* **46**, 4971 (2011).
22. W.D. Liu, K.X. Liu, X.X. Xia, and W.H. Wang: The failure stress of bulk metallic glasses under very high strain rate. *J. Mater. Res.* **25**, 1230 (2010).
23. F. Sadeghi, A. Kermanpur, N. Sarami, D. Heydari, J. Nematollahi, and M. Bahmani: A comparison on the EBSD and RO-XRD techniques for measuring crystal orientation of the single-crystal

https://doi.org/10.1557/jmr.2018.251 Published online by Cambridge University Press

Ni-Based superalloys. *Metallogr., Microstruct., Anal.* **5**, 342 (2016).
24. Z. Guo, T. Fu, and H. Fu: Crystal orientation measured by XRD and annotation of the butterfly diagram. *Mater. Charact.* **44**, 431 (2000).
25. Z.M. Xu, Z.Q. Guo, and J.G. Li: A new method to evaluate the quality of single crystal Cu by an X-ray diffraction butterfly pattern method. *Mater. Charact.* **53**, 395 (2004).
26. C.B. Yang, L. Liu, X.B. Zhao, Y.F. Li, J. Zhang, and H.Z. Fu: Dendrite morphology and evolution mechanism of nickel-based single crystal superalloys grown along the ⟨001⟩ and ⟨011⟩ orientations. *Prog. Nat. Sci.: Mater. Int.* **22**, 407 (2012).
27. Z.Q. Wang, I.J. Beyerlein, and R. LeSar: Plastic anisotropy in fcc single crystals in high rate deformation. *Int. J. Plast.* **25**, 26 (2009).
28. S.S. Ezz, Y.Q. Sun, and P.B. Hirsch: Strain rate dependence of the flow stress and work hardening of γ'. *Mater. Sci. Eng., A* **192–193**, 45 (1995).
29. W. Österle, D. Bettge, B. Fedelich, and H. Klingelhöffer: Modelling the orientation and direction dependence of the critical resolved shear stress of nickel-base superalloy single crystals. *Acta Mater.* **48**, 689 (2000).
30. D.M. Shah and D.N. Duhl: The effect of orientation, temperature and gamma prime size on the yield strength of a single crystal nickel base superalloy. In *Superalloys*, W.B.K.R.H. Bricknell, M. Gell, C.S. Kortovich, and J.F. Radavich, eds. (TMS, Warrendale, Pennsylvania, 1984); p. 105.
31. E.F. Westbrooke, L.E. Forero, and F. Ebrahimi: Slip analysis in a Ni-base superalloy. *Acta Mater.* **53**, 2137 (2005).
32. P. Li, B.M. Zhou, Y.Z. Zhou, J.G. Li, T. Jin, X.F. Sun, and Z.F. Zhang: Effect of orientations on in situ tensile deformation and fracture behaviours of nickel-base single-crystal superalloys. *Philos. Mag. A* **94**, 2426 (2014).
33. R. Miner, T. Gabb, J. Gayda, and K. Hemker: Orientation and temperature dependence of some mechanical properties of the single-crystal nickel-base superalloy René N_4: Part III. Tension-compression anisotropy. *Metall. Mater. Trans. A* **17**, 507 (1986).
34. A. Nitz, U. Lagerpusch, and E. Nembach: CRSS anisotropy and tension/compression asymmetry of a commercial superalloy. *Acta Mater.* **46**, 4769 (1998).
35. C. Lall, S. Chin, and D.P. Pope: The orientation and temperature dependence of the yield stress of Ni_3(Al,Nb) single crystals. *Metall. Trans. A* **10**, 1323 (1979).

https://doi.org/10.1557/jmr.2018.251 Published online by Cambridge University Press